Electronic Supplementary Information (ESI)

Cs-substituted tungstophosphate-supported ruthenium nanoparticles as efficient and robust bifunctional catalysts for the conversions of inulin and cellulose into hexitols in water in the presence of H_2

Weiping Deng, Enze Zhu, Mi Liu, Qinghong Zhang and Ye Wang*

State Key Laboratory of Physical Chemistry of Solid Surfaces, Collaborative Innovation Center of Chemistry for Energy Materials, National Engineering Laboratory for Green Productions of Alcohols, Ethers and Esters, College of Chemistry and Chemical Engineering, Xiamen University.

** Corresponding author*

Fax: +86 592 2183048; Tel: +86 592 2186156; E-mail: wangye@xmu.edu.cn

1. XRD patterns of $Cs_xH_{3-x}PW_{12}O_{40}$ and Ru/$Cs_xH_{3-x}PW_{12}O_{40}$ catalysts with different Cs contents

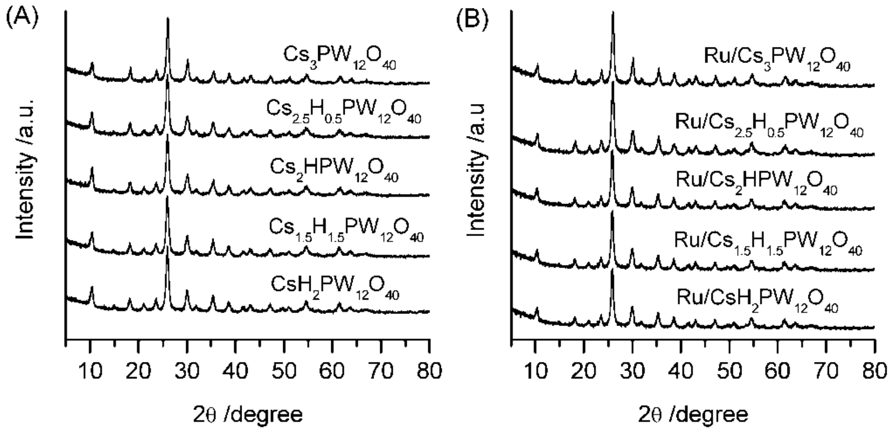

Fig. S1 XRD patterns. (A) $Cs_xH_{3-x}PW_{12}O_{40}$, (B) Ru/$Cs_xH_{3-x}PW_{12}O_{40}$ catalysts.

2. N_2 adsorption-desorption isotherms of $Cs_xH_{3-x}PW_{12}O_{40}$ samples with different Cs contents

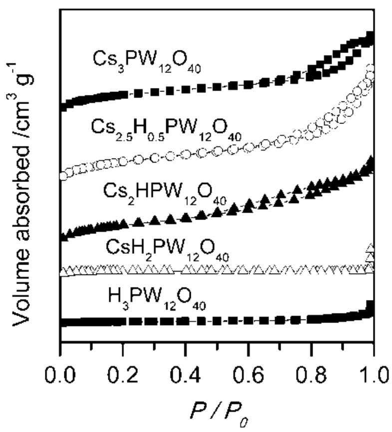

Fig. S2 N_2 adsorption-desorption isotherms of $Cs_xH_{3-x}PW_{12}O_{40}$ samples with different Cs contents at 77 K.

3. Ru 3d XPS spectra for Ru/$Cs_xH_{3-x}PW_{12}O_{40}$ catalysts with different Cs contents

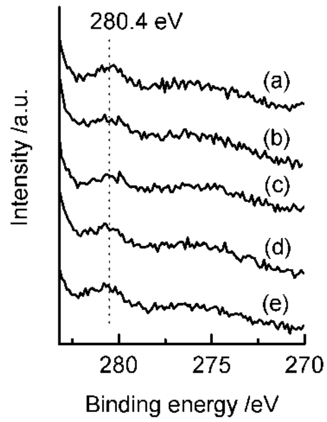

Fig. S3 Ru 3d XPS spectra for Ru/$Cs_xH_{3-x}PW_{12}O_{40}$ catalysts with different Cs contents. (a) x = 1.0; (b) x = 1.5; (c) x = 2.0; (d) x = 2.5; (e) x =3.0.

4. Typical TEM micrograph and particle size distribution for colloidal Ru nanoparticles synthesized by the reduction of $RuCl_3$ with ascorbic acid

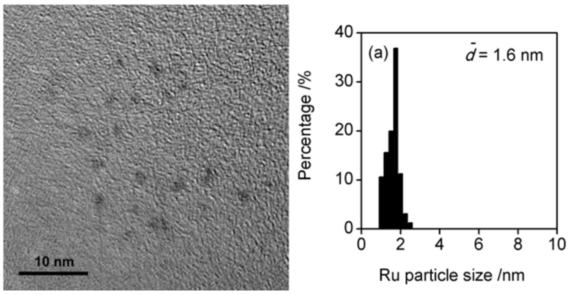

Fig. S4 Typical TEM micrograph and the particle size distribution for the colloidal Ru nanoparticles synthesized by the reduction of $RuCl_3$ with ascorbic acid.

5. NH_3-TPD profiles and some physicochemical properties for several typical solid acids

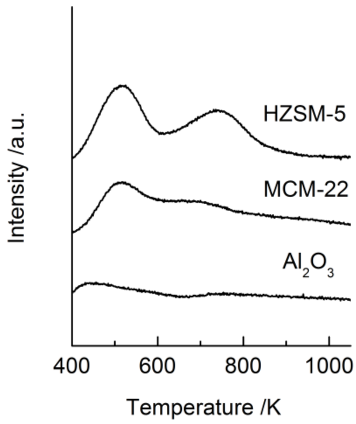

Fig. S5 NH_3-TPD profiles for H-ZSM-5, MCM-22 and Al_2O_3.

Table S1 Some physicochemical properties of solid acids

Catalyst	NH_3 desorption amount at 400-600 K (mmol g^{-1})	NH_3 desorption amount at 600-850 K (mmol g^{-1})	Micropore size (nm)	Mesopore size (nm)
HZSM-5	0.38	0.35	0.55	-
MCM-22	0.27	0.15	0.70	-
Al_2O_3	0.11	0.01	-	7.0

6. TEM micrographs and particle size distributions for Ru nanoparticles loaded on several supports

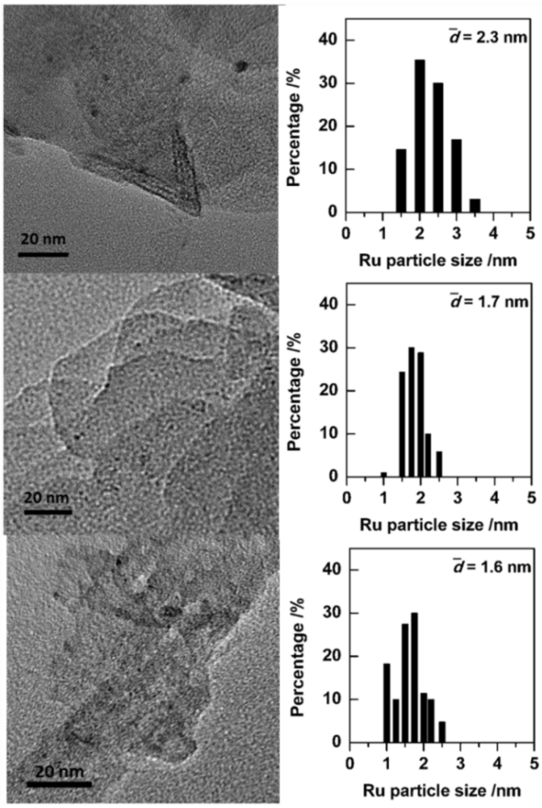

Fig. S6 Typical TEM micrographs and particle size distributions for Ru nanoparticles loaded on several supports. (a) HZSM-5, (b) MCM-22, (c) Al_2O_3.

7. XRD patterns, XPS spectra and some properties for the $Ru/Cs_3PW_{12}O_{40}$ catalyst before and after reaction

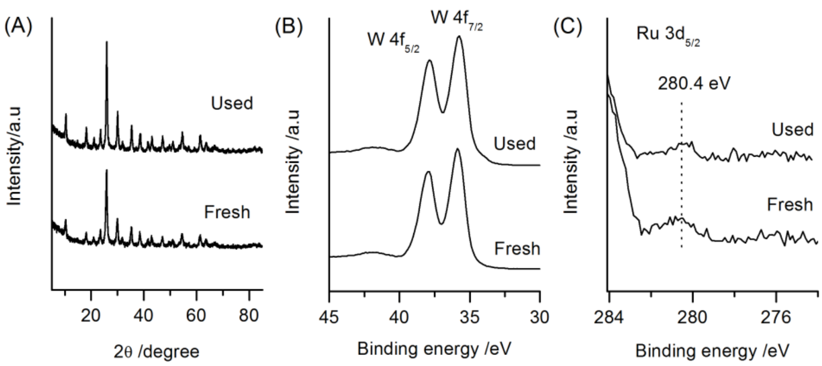

Fig. S7 (A) XRD patterns for $Ru/Cs_3PW_{12}O_{40}$ catalyst. (B) W 4f XPS spectra and (C) Ru 3d XPS spectra for $Ru/Cs_3PW_{12}O_{40}$ catalyst.

Table S2 Some physicochemical properties of Ru catalyst before and after 5 recycling uses.

$Ru/Cs_{3.0}PW_{12}O_{40}$	Ru leaching[a] (ppm)	*D*(Ru)[b]	*d*(Ru)[c] (nm)
Fresh	-	0.49	1.9
Used	< 0.1	0.24	3.7

[a]The amounts of Ru leached into the solution were measured by ICP-MS. [b]*D*(Ru) denotes the Ru dispersion obtained from CO chemisorption. [c] *d*(Ru) denotes the size of Ru particles estimated from *D*(Ru) by using $d(\mathrm{Ru}) = 6V_m/[D(\mathrm{Ru})\times a_m]$ (nm).

8. Pyridine-adsorbed FT-IR spectra for $Cs_3PW_{12}O_{40}$ under H_2 with different pressures

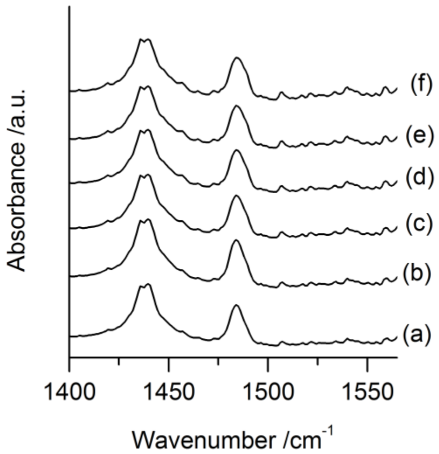

Fig. S8 Pyridine-adsorbed FT-IR spectra for $Cs_3PW_{12}O_{40}$ under H_2 with different pressures at 323 K. (a) At 323 K after pretreatment in H_2 at 573 K followed by evacuation. (b)-(f) Under H_2 with different pressures: (b)12.8 kPa, (c) 19.2 kPa, (d) 25.6 kPa, (e) 33.3 kPa, (f) 44.8 kPa.

9. Pyridine-adsorbed FT-IR spectra for Ru/Al_2O_3 under H_2 with different pressures

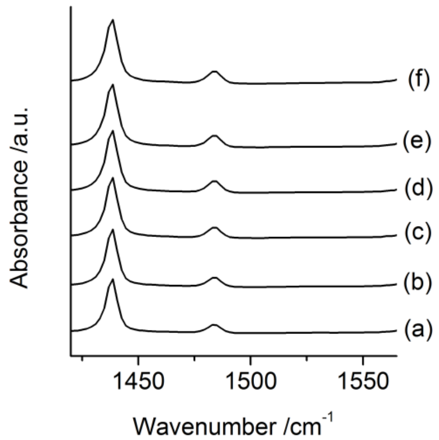

Fig. S9 Pyridine-adsorbed FT-IR spectra for Ru/Al_2O_3 under H_2 with different pressures at 323 K. (a) At 323 K after pretreatment in H_2 at 573 K followed by evacuation. (b)-(f) Under H_2 with different pressures: (b) 12.8 kPa, (c) 19.2 kPa, (d) 25.6 kPa, (e) 33.3 kPa, (f) 44.8 kPa.

10. Raman spectra for $Cs_3PW_{12}O_{40}$ under N_2 and H_2 atmospheres at 423 K

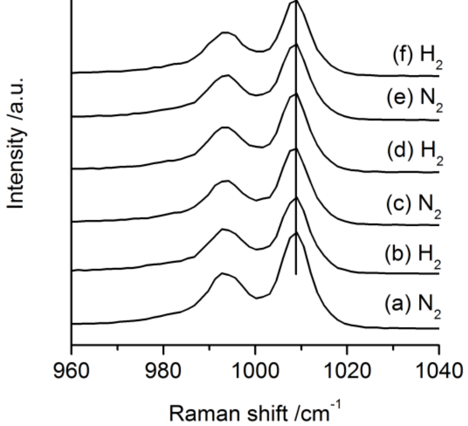

Fig. S10 Raman spectra for $Cs_3PW_{12}O_{40}$ under N_2 and H_2 atmospheres at 423 K.(a) After the introduction of N_2 into the pretreated sample, (b) 10 min after switching to H_2, (c) 10 min after switching again to N_2, (d) 10 min after switching again to H_2, (e) 10 min after switching again to N_2, (f) 10 min after switching again to H_2.

11. TEM micrographs and particle size distributions for colloidal Ru nanoparticles synthesized by reducing $RuCl_3$ with ascorbic acid under different conditions

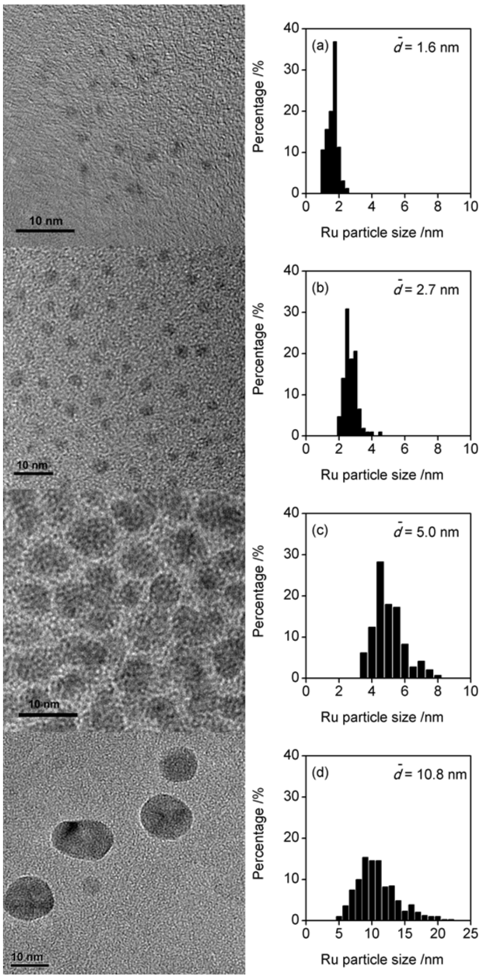

Fig. S11 TEM micrographs and particle size distributions for colloidal Ru nanoparticles with different mean sizes synthesized by reducing $RuCl_3$ with ascorbic acid under different conditions. See Table 3 for synthetic conditions.

12. Fructose conversions over the $Ru/Cs_3PW_{12}O_{40}$catalysts with different mean sizes of Ru particles

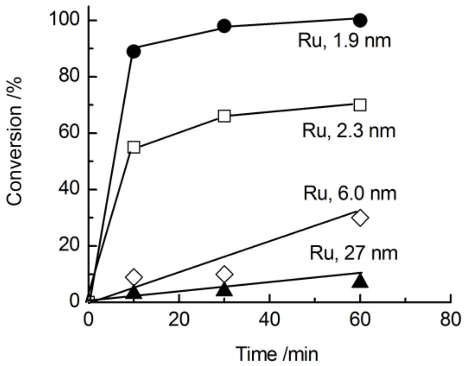

Fig. S12 Fructose conversions over the $Ru/Cs_3PW_{12}O_{40}$ catalysts with different mean sizes of Ru nanoparticles. Reaction conditions: fructose, 110 mmol L^{-1}; H_2O, 10 mL; $P(H_2)$ = 2 MPa; T = 363 K.

13. Turnover frequency (TOF) for the hydrogenation of fructose to hexitols over the $Ru/Cs_3PW_{12}O_{40}$ catalysts with different mean sizes of Ru particles

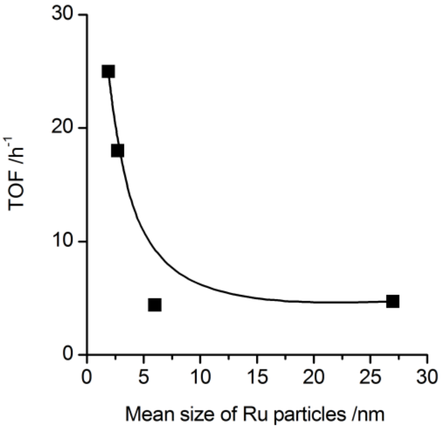

Fig. S13 TOF for the hydrogenation of fructose to hexitols over the $Ru/Cs_3PW_{12}O_{40}$ catalysts with different mean sizes of Ru particles. Reaction conditions: fructose, 110 mmol L^{-1}; H_2O, 10 mL; $P(H_2)$ = 2 MPa; T = 363 K.